Supplementary Information (SI) for Nanoscale.
This journal is © The Royal Society of Chemistry 2026

Supporting Information

Operando TEM study of a working TiO_2 supported Au and Au–Cu catalysts during butadiene hydrogenation

Abdallah Nassereddine,*[a,b] Laurent Delannoy,†[c] Catherine Louis,[c] Guillaume Wang,[a] Damien Alloyeau,[a] Christian Ricolleau,[a] Axel Wilson [a] and Jaysen Nelayah*[a]

[a.] *Université Paris Cité, CNRS, Laboratoire Matériaux et Phénomènes Quantiques, 75013 Paris, France*
[b.] *Present adress : Institut Néel, UPR 2940 CNRS- Université Grenoble Alpes, Grenoble F-38000, France*
[c.] *Sorbonne Université, CNRS, Laboratoire de Réactivité de Surface, LRS, F-75005 Paris, France*
† Dr. Laurent Delannoy deceased May 12, 2024.

S1. Operando ETEM implementation

- ***Coupling ETEM with Mass Spectrometry for Real-Time Catalytic Monitoring***

Mass spectrometric analysis of the reaction effluent was carried out using a Pfeiffer Vacuum "PrismaPro QMG 250 F1" Residual Gas Analyzer (RGA). This instrument covered the mass-to charge ratio (m/z) range of 1–100 amu. During butadiene hydrogenation, the RGA primarily detects the parent ions of the reactants and reaction products, namely:

- H_2^+ at m/z = 2 amu
- He^+ at m/z = 4 amu
- $C_4H_6^+$ at m/z = 54 amu (butadiene)
- $C_4H_8^+$ at m/z = 56 amu (butenes)
- $C_4H_{10}^+$ at m/z = 58 amu (butane)

In addition to these parent ions, fragmentation due to 70 eV electron bombardment in the analyzer ion source produces lighter fragment ions. The RGA ion source consists of an iridium filament coated with Y_2O_3, heated to around 1300 °C by the Joule effect. At such high temperatures, mild degassing of source components and surrounding surfaces can introduce trace signals from air constituents (H_2O, O_2, N_2, and CO_2). Although these appear in the RGA spectra, they are typically in very low abundance. Table S1 compiles the parent-ion m/z values for the main components in our reaction mixture (H_2, He, C_4H_6, C_4H_8, C_4H_{10}) alongside those of air (O_2, N_2) and other minor species. Because the RGA does not distinguish between the various butene isomers (1-butene, cis-2-butene, trans-2-butene), all butene products are grouped under the general label C_4H_8.

Table S1. Mass spectrometric signatures of reactants, products and background gases during butadiene hydrogenation

Reactants and gas products	Empirical formula	Parents ion	m/z	Principal fragments	m/z
Hydrogen	H_2	H_2^+	2	H^+	1
Helium	He	He^{2+}	4	He^+	3
Butadiene	C_4H_6	$C_4H_6^+$	54	$C_4H_5^+$, $C_3H_3^+$	53,39
Butenes	C_4H_8	$C_4H_8^+$	56	$C_3H_5^+$	41
Butane	C_4H_{10}	$C_4H_{10}^+$	58	$C_3H_7^+$	43
Water vapour	H_2O	H_2O^+	18	H_2^+, HO^+, O^+	2, 17, 16

Nitrogen	N_2	N_2^+	28	N^+	14
Carbon monoxide	O_2	O_2^+	32	O^+	16
Carbon dioxide	CO_2	CO_2^+	44	CO^+, O^+, C^+	28, 16, 12

- ***Pre-analysis purge and typical RGA spectra***

Before each RGA measurement, the high-pressure Protochips Atmosphere cell and gas lines were purged for 30 minutes with pure Ar, followed by 20 minutes under the butadiene hydrogenation mixture (20% H_2/0.36% C_4H_6/79.64% He) at atmospheric pressure and 120 °C. This initial purge at 120 °C helps eliminate residual solvent (mainly water) from the catalyst suspension, preventing contamination of the E-chip. Figure S1.A shows a typical mass spectrum acquired in full scan mode (m/z = 1–100) after 20 minutes of purging Au/TiO_2 catalysts under our reaction mixture. The ion-counting dwell time was 32 ms per channel. Peaks for parent ions and their fragments appear at m/z values corresponding to H_2, He, and C_4H_6, as well as minor signals for residual Ar from the initial inert purge. The intensity of the butane (C_4H_{10}) peak at 120 °C was very low, near the RGA detection limit (~10^{-14} to 10^{-15} A), and is thus omitted from subsequent analyses.

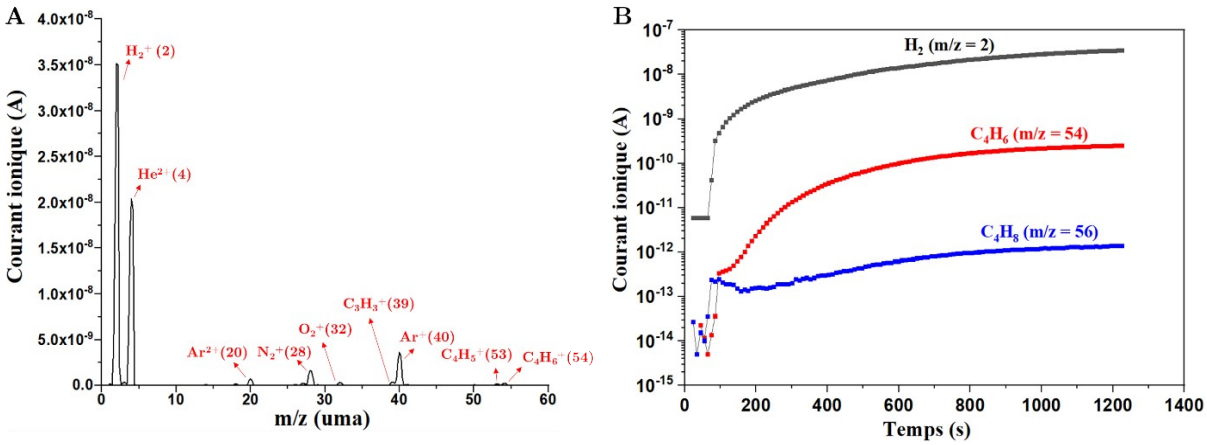

Figure S1. (A) Mass spectrum in scan mode after 20 minutes of purging at atmospheric pressure with the butadiene hydrogenation gas mixture (20% H_2 / 0.36% C_4H_6 / 79.64% He) at 120 °C. (B) Time-resolved monitoring in Bin mode of the ion current intensities corresponding to the key species involved in the butadiene hydrogenation reaction: H_2 (m/z = 2) and C_4H_6 (m/z = 54) as reactants, and C_4H_8 (m/z = 56) as product. The temporal evolution of these intensities indicates stabilization of the reactive gas mixture after approximately 20 minutes of purging, with a large H_2 excess relative to C_4H_6 (H_2/C_4H_6 ≈ 100), and the concurrent formation of a small amount of C_4H_8.

Traces of N_2 (m/z = 28) and O_2 (m/z = 32) from ambient air leakage into the RGA are also visible. However, they do not interfere significantly with detecting the key ions C_4H_6+ (m/z = 54) and $C_4H_8^+$ (m/z = 56). The baseline RGA pressure during these measurements was on the order of 3.5×10^{-5} mbar. It should be noted that the RGA signal intensities of different molecules cannot be directly compared as absolute molar abundances. In particular, butadiene contributes not only to its parent ion at m/z = 54 but also to fragment ions under 70 eV electron-impact ionization, while part of the signals at m/z = 28 and 32 originates from residual background contributions in the RGA environment, including outgassing of the hot ion source and adjacent chamber walls [1].

For semi-quantitative kinetic monitoring (bin mode), we measured the time evolution of molecular hydrogen (m/z = 2), butadiene (m/z = 54), and butenes (m/z = 56). The dwell times were set to 4096 ms for H_2^+ and $C_4H_6^+$, and 8192 ms for $C_4H_8^+$, which has a lower expected concentration. As shown in Figure S1.B, 20 minutes of purging at 120 °C under the reactive gas flow was sufficient to reach a stable mixture composition.

S2. Particle-size analysis of Au/TiO₂ before and after catalytic testing

The mean particle size was calculated as the Sauter mean diameter $d32 = \sum nidi^3/nidi^2$, which is more relevant for catalytic systems than the simple arithmetic mean because it accounts for the surface-volume contribution of the nanoparticles [2].

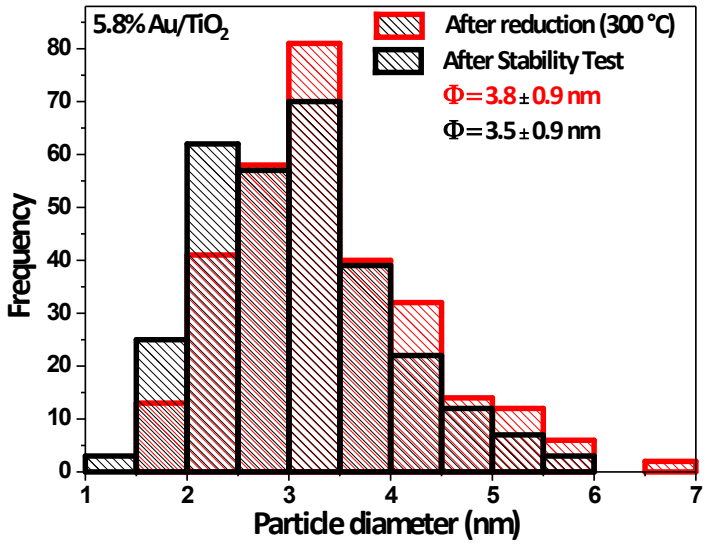

Figure S2. Ex situ particle-size distributions of Au/TiO_2 nanoparticles measured after synthesis and after catalysis. The mean particle size was calculated using the Sauter mean diameter, $d32=\sum nidi^3/\sum nidi^2$. The resulting values are 3.8 ± 0.9 nm after synthesis and 3.5 ± 0.9 nm after catalysis, confirming the high structural stability of Au/TiO_2 under butadiene hydrogenation conditions.

- ***Comparison with laboratory-scale catalytic tests***

Although *operando* ETEM coupled with mass spectrometry provides direct insights into catalyst structure–reactivity relationships under reaction conditions, it is important to note that these microscopic investigations do not replicate all aspects of typical laboratory-scale catalytic tests. Several factors limit a direct comparison of catalytic performance metrics:

1. Catalyst mass

Laboratory-scale reactors often use tens to hundreds of milligrams of catalyst, whereas an *operando* ETEM experiment may employ only a few nanograms. This vast difference in catalyst loading influences gas–solid contact times, making quantitative comparisons challenging.

2. Reactor geometry

Conventional lab reactors typically use fixed-bed or continuous-flow tubular geometries, whereas the TEM holder high-pressure cell more closely resembles a horizontal “trickle-bed” system. Variations in flow patterns and contact times can significantly impact observed reaction kinetics.

3. Gas flow control

While the ETEM setup allows precise control of the gas composition, it often lacks mass flow controllers to accurately measure flow rates. In contrast, standard laboratory reactors typically have well-calibrated flow systems, ensuring reproducible and quantifiable gas-solid interaction times.

4. Heating uniformity

In many lab reactors, a well-designed furnace maintains a uniform temperature across the entire catalyst bed. By contrast, ETEM uses a microheater chip (e.g., SiC membrane of a few hundred micrometers squared), potentially creating thermal gradients. These local temperature variations can affect reaction rates and observed structures.

5. Activation procedure

Laboratory reactors commonly include an *in situ* reduction step (e.g., under hydrogen at 300 °C) immediately before the reaction. In an ETEM experiment, catalysts may undergo *ex situ* reduction and then be exposed to air during transfer into the microscope. Although this approach ensures initial structures are well-defined for *in situ* observation, it differs from continuous *in situ* reduction protocols used in many lab-scale studies.

Because of these differences in catalyst mass, reactor geometry, flow control, heating, and activation, absolute reaction rates or conversions measured in an ETEM environment cannot be directly compared with those from larger-scale tests. Nevertheless, the high-resolution, real-time structural information gained from *operando* ETEM experiments offers valuable mechanistic insights that complement bulk catalytic data and can guide the optimization of catalysts for industrial applications.

S3. First-approximation estimate of Au and Cu adatom detachment barriers during Ostwald ripening

Following the first-approximation approach proposed by Alloyeau *et al.* [3], the adatom detachment/evaporation barrier is estimated as:

$\Delta E \approx E_a - E_c$

Where:

ΔE is the estimated detachment barrier (eV),

E_a is the adsorption energy of an adatom on the TiO_2 surface (in eV)

E_c = cohesive energy of the bulk metal (in eV/atom)

To apply this expression consistently, Ea and Ec must be written using the same sign convention. In the present work, all energies were written with the isolated atom taken as the reference state, following the convention used by Alloyeau *et al.* [3].

The cohesive energies used are [4]:

$Ec(Au) = -3.81\ eV/atom$

$Ec(Cu) = -3.49\ eV/atom$

For Au, the adsorption energies taken from Yuan *et al.* study [5] are already reported with the negative sign for exothermic adsorption:

$Ea(Au,101) = -0.54\ eV$

$Ea(Au,001) = -2.74\ eV$

For Cu, Seriani *et al.* [6] reports adsorption energies as positive binding energies because the adsorption-energy expression contains an overall minus sign. Therefore, for consistency with the signed convention used in the present calculation, these values were rewritten as negative adsorption energies:

$Ea(Cu,101) = -2.30\ eV$

$Ea(Cu,001) = -2.83\ eV$

The estimated barriers are then:

<u>On TiO_2 (101) surface:</u>

- For Au:
  $\Delta E = E_a - E_c = -0.54\ eV - (-3.81)\ eV = 3.27\ eV$

- For Cu:

$$\Delta E = E_a - E_c = -2.30\ eV - (-3.49\ eV) = 1.19\ eV$$

On TiO_2 (001) surface:

- For Au:
$$\Delta E = E_a - E_c = -2.74\ eV - (-3.81)\ eV = 1.07\ eV$$

- For Cu:

$$\Delta E = E_a - E_c = -2.83\ eV - (-3.49)\ eV = 0.66\ eV$$

S4. Deposition-precipitation with urea synthesis steps of Au and Au-Cu/TiO_2 catalysts

Figure S3. Schematic representation of the deposition–precipitation with urea (DPU) synthesis steps for monometallic Au and bimetallic AuCu catalysts supported on TiO_2. Briefly, TiO_2 is dispersed in water, then mixed with the appropriate amount of metal precursors ($HAuCl_4 \cdot 3H_2O$ and/or $Cu(NO_3)_2 \cdot 3H_2O$) and urea at 80 °C. After 20 h of stirring, the resulting precipitate is separated by washing and centrifugation, dried under vacuum at room temperature, and finally thermally treated under H_2 (300 °C) to obtain the final catalysts.

S5. Schematic Illustration of the operando TEM Setup

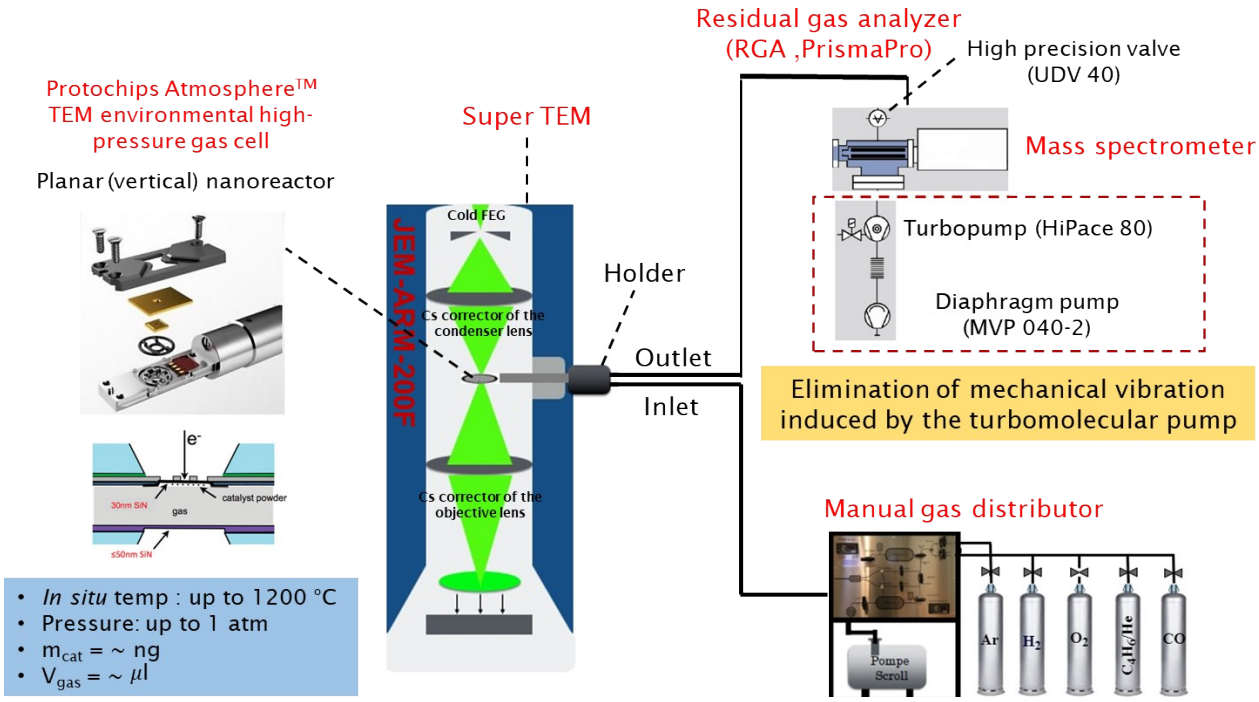

Figure S4. Schematic representation of the JEOL ARM-200F double aberration-corrected microscope coupled with the Protochips Atmosphere™ high-pressure gas cell and a PrismaPro residual gas analyzer (RGA) for *operando* measurements. The sample environment is controlled via a manual gas distributor, while mechanical vibrations from the turbomolecular pump are minimized. The inset highlights the E-chip configuration, with 30–50 nm thick SiN windows allowing electron transparency at pressures up to 1 atm and temperatures up to 1200 °C.

References

[1] Stanford Research Systems, choosing a Quadrupole Gas Analyzer, https://www.thinksrs.com/downloads/pdfs/applicationnotes/cis.pdf, (accessed 25 March 2026).

[2] Haramkar, S. S., Thombre, G. N., Jadhav, S. V., & Thorat, B. N. (2021). Comptes Rendus. Chimie, 24(2), 255-265.

[3] D. Alloyeau, G. Prévot, Y. Le Bouar, T. Oikawa, C. Langlois, A. Loiseau and C. Ricolleau, Phys. Rev. Lett., 2010, 105, 255901.

[4] C. Kittel, Introduction to solid state physics, Wiley, Hoboken, NJ, 8. ed., [repr.]., 20.

[5] W. Yuan, D. Zhang, Y. Ou, K. Fang, B. Zhu, H. Yang, T. W. Hansen, J. B. Wagner, Z. Zhang, Y. Gao and Y. Wang, Angewandte Chemie, 2018, 130, 17069–17073.

[6] N. Seriani, C. Pinilla and Y. Crespo, J. Phys. Chem. C, 2015, 119, 6696–6702.